metals

MDPI

Article

Structural Integrity Assessment of Independent Type-C Cylindrical Tanks Using Finite Element Analysis: Comparative Study Using Stainless Steel and Aluminum Alloy

Young-IL Park, Jin-Seong Cho and Jeong-Hwan Kim *

Department of Naval Architecture and Offshore Engineering, Dong-A University, Busan 49315, Korea; parkyi1973@dau.ac.kr (Y.-I.P.); 1532897@donga.ac.kr (J.-S.C.)
* Correspondence: jhkim81@dau.ac.kr

Abstract: The International Maritime Organization stipulates that greenhouse gas emissions from ships should be reduced by at least 50% relative to the amount observed in 2008. Consequently, the demand for liquefied natural gas (LNG)-fueled ships has increased significantly. Therefore, an independent type-C cylindrical tank, which is typically applied as an LNG fuel tank, should be investigated. In this study, structural integrity assessments using finite element analysis are performed on C-type LNG fuel tanks for a sea-cleaning vessel. In addition, the applicability of stainless steel and aluminum alloys is evaluated for LNG tank construction. Structural analyses and fatigue limit evaluations, including heat transfer analyses for the tank based on IGC code requirements, are performed, and the results are compared. The results of this study are expected to facilitate the selection of materials used for independent type-C tanks.

Keywords: independent type-C cylindrical tank; LNG fuel tank; structural integrity assessment; finite element analysis; IGC code

Citation: Park, Y.-I.; Cho, J.-S.; Kim, J.-H. Structural Integrity Assessment of Independent Type-C Cylindrical Tanks Using Finite Element Analysis: Comparative Study Using Stainless Steel and Aluminum Alloy. *Metals* **2021**, *11*, 1632. https://doi.org/10.3390/met11101632

Academic Editors: Matteo Benedetti and Denis Benasciutti

Received: 30 August 2021
Accepted: 8 October 2021
Published: 14 October 2021

1. Introduction

Liquefied natural gas (LNG), as a bunker fuel, can reduce atmospheric pollution. Compared with traditional fuels such as heavy fuel oil, LNG emits significantly lower amounts of sulfur oxides, nitrogen oxides, and particulate matter. In particular, the International Maritime Organization (IMO) stipulates that greenhouse gas emissions from ships should be reduced by at least 50% relative to the amount observed in 2008. Therefore, the demand for LNG-fueled ships has increased significantly [1].

The IMO classifies LNG tanks into two systems: an integrated tank system and an independent self-supporting tank system. The integrated tank system is surrounded by a complete hull structure. The structure members of the tank participate in the overall hull strength because the hull and tank are integrated. Independent self-supporting tank systems can be classified into types A, B, and C based on the type and presence of a secondary barrier. Type-A and type-B tanks require a complete secondary barrier and a partial secondary barrier, respectively, whereas the type-C tanks require no secondary barrier. Among them, the type-C tank is designed as a pressure vessel that can withstand high vapor pressures, thereby precluding the risk of leakage during the tank's lifetime; consequently, no secondary barrier is required. Therefore, it is suitable as a fuel tank for ships because of its simple design, low cost, and high safety [2].

Most LNG-fueled tanks are constructed using stainless steel and aluminum alloys [3,4]. They do not cause brittle fracture at extremely low temperatures, rendering them suitable for storing LNG at −163 °C. However, each material has its advantages/disadvantages and is applied differently depending on the purpose. Stainless steel offers good chemical resistance; therefore, it can easily reduce the contamination hazards of cargo and offers good corrosion resistance. SUS316L contains less carbon than SUS316. Here, "L" represents

"low", and low carbon contents can improve corrosion resistance near welds. SUS304 and SUS304L are similar to SUS316 and SUS316L, respectively, in terms of their properties; however, SUS304 and SUS304L are cheaper. Aluminum offers many advantages over stainless steel from the perspective of ship construction. Aluminum alloys are lighter than steel alloys (the density of aluminum alloy is 2.66 tonnes/m^3 and that of steel alloy is 7.85 tonnes/m^3); therefore, using an aluminum structure can reduce the weight by 65% compared with using a steel structure. Consequently, the vessel can afford a higher load capacity and lower displacement [5,6].

Recent studies pertaining to membrane-type or independent type-B tanks are relatively abundant [7–13]. Kim et al. proposed a procedure for structural integrity evaluation of a type-B LNG fuel tank based on the International Code of the Construction and Equipment of Ships Carrying Liquefied Gases in Bulk (IGC code). They conducted a series of finite element analyses under various design loads and evaluated the structural safety of the tank [7]. Park developed the ultimate crushing strength criteria for a membrane-type cargo containment system under sloshing load. He also utilized the finite element method to evaluate the crushing strength of the cargo containment system and compared the results with DNV guidance [12]. However, studies regarding the design of type-C tanks are scarce [14–16]. Lin et al. proposed an approach for evaluating the boil-off rate (BOR) of LNG in a type-C tank under different filling ratios. They estimated the BOR based on the finite element analysis and compared the results with experimental measurements [14]. Heo et al. reviewed the rule scantling process and calculation methods of the IGC Code and evaluated the structural safety of a type-C tank based on the IGC Code [15]. It was assumed that type-C tanks are primarily applied to small ships and afford relatively high safety. In this study, structural integrity assessments were performed on C-type LNG fuel tanks, which were constructed using stainless steel and aluminum alloys, for a sea-cleaning vessel. Structural analyses and fatigue limit evaluations, including heat transfer analyses for the tank based on the IGC code requirements, were performed, and the results were compared. The results of this study are expected to facilitate the selection of materials for independent type-C tanks.

2. Procedure of Structural Integrity Assessment for Independent Type-C Cylindrical Tanks

The calculation procedure for the structural integrity assessment of the independent type-C cylindrical tank applied in this study is presented in Figure 1. The entire methodology can be segmented into three stages, i.e., heat transfer analysis, structural analysis, and fatigue analysis, and is based on the IGC Code and KR rules [2,17]. Because LNG is stored in a liquid state at −163 °C, the thermal effect due to the temperature difference from the ambient temperature must be considered in the evaluation. Therefore, the structural analysis that follows includes the thermal distribution of the structure derived from the heat transfer analysis. In this study, three structural analyses, i.e., those based on the maximum acceleration conditions under normal operating conditions, 30° heeled conditions, and collision conditions, were performed for the structural assessment. Fatigue analysis was performed while considering the stress of the structure derived through structural analysis and the number of cycles for a specific scenario. For fatigue analysis, high-cycle fatigue analyses under normal operating conditions and low-cycle fatigue analyses in bunkering conditions were performed. Although the numbers of loadings and unloadings generated during the bunkering process are low, the low-cycle fatigue analysis method is typically used because a high stress range is expected owing to the temperature difference.

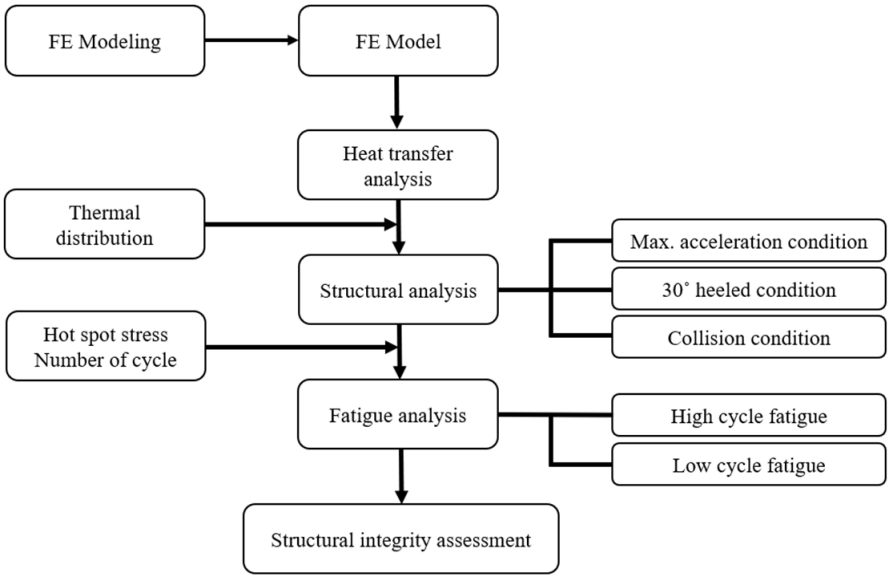

Figure 1. Flow chart of structural integrity assessment for independent type-C cylindrical tank applied in this study.

3. Target Vessel

The target vessel of this study was an LNG-fueled sea-cleaning vessel for collecting and cleaning buoyant ocean trash waste. The general configuration of the ship and the location of the LNG tank with a volume of 15 m^3 are illustrated in Figure 2. The specifications of the target vessel with the LNG tank are listed in Table 1.

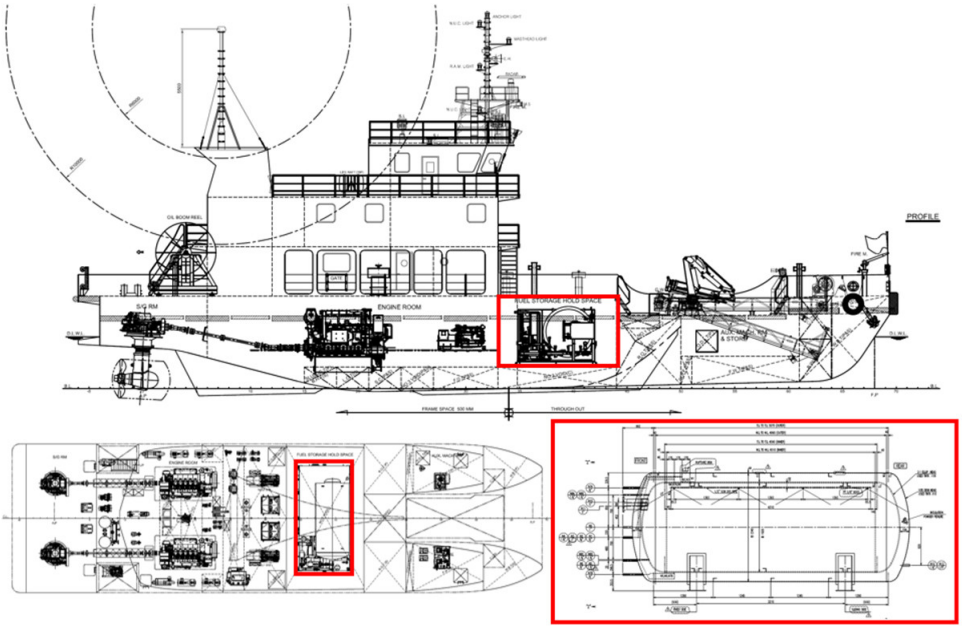

Figure 2. General configuration of target ship and location of LNG fuel tank.

Table 1. Specifications of target vessel with type-C cylindrical tank.

L (m)	C_B	B (m)	x (m)	y (m)	z (m)	V (knot)	K	ρ (kg/m^3)
34	0.662	10.6	12.5	0.092	−0.079	12.5	5.0	500

In the table above, L is the length of the vessel for the scantlings, C_B the block coefficient, B the ship breadth, x the longitudinal distance from the midship to the center of gravity of the tank, y the transverse distance from the centerline to the center of gravity of the tank, z the vertical distance from the waterline to the center of gravity of the tank, V the service speed of the ship, and K = 1 in general. For particular cases, K is calculated as $\frac{13\overline{GM}}{B}$, where $\overline{GM}$ is the metacentric height (m), and ρ the density of LNG.

4. Numerical Modeling

4.1. Finite Element Model

Figure 3 shows the geometry of the LNG fuel tank. The tank comprises an inner tank and an outer tank. Because the inner tank is used to contain LNG, it was manufactured using materials that exhibit good cryogenic performance. In this study, two types of stainless steel alloys (SUS304 and 304L) and Al-5083-O were used for modeling and evaluation. SUS316/316L were not considered in the calculation because their material properties are the same as those of SUS304/304L. The outer tank was constructed using carbon steel DH32. The inner and outer tanks were connected with Bakelite supports (Bakelite is a type of insulation material made from synthetic components) [18]. The entire tank was mounted on two saddles, and the outer tank and saddle were attached by welding.

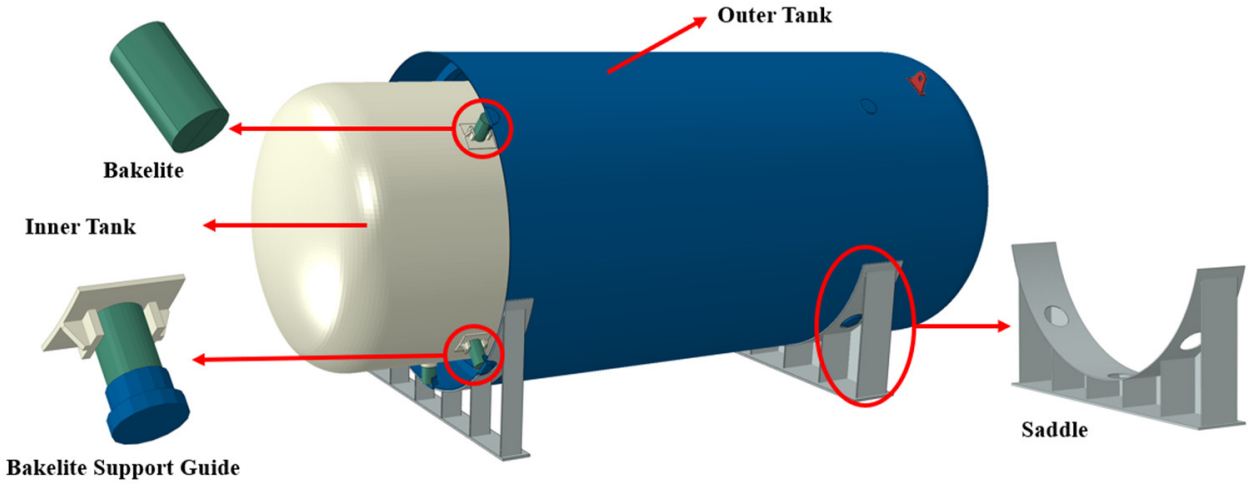

Figure 3. Geometry of LNG fuel tank.

Figure 4 shows the finite element model of the target LNG fuel tank made with ABAQUS/Standard 6.14 software [19]. All components of the tank, such as the inner tank, outer tank, Bakelite support, and saddle, were discretized using solid (C3D8R) elements. Here, the C3D8R element was a reduced integrated eight-node linear brick element with hourglass control [19]. The surface-to-surface penalty contact condition was considered for inner and outer tanks in the FE model. Two elements in the thickness direction were used to model the structural members to implement the bending behavior. The element size was set to be less than three times the element thickness. In other words, because the thickness of the inner tank shell was 15 mm (i.e., the element thickness was 7.5 mm), the size of all elements did not exceed 22.5 mm. The numbers of elements and nodes were 238,118 and 357,259, respectively. The materials used for modeling are listed in Table 2.

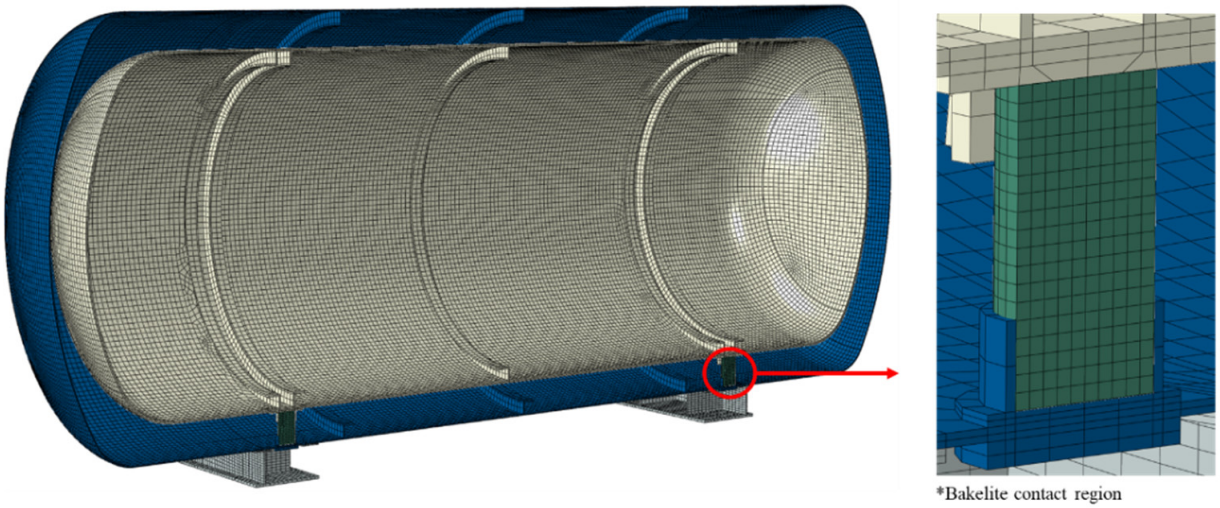

Figure 4. Finite element model of LNG fuel tank.

Table 2. Mechanical and thermal properties of target materials.

Parameter	Carbon Steel DH36	SUS304	SUS304L	AL 5083-O	Bakelite
Poisson's ratio	0.30	0.29	0.29	0.33	0.29
Elastic modulus (MPa)	205,800	193,000	193,000	71,000	8300
Density (tonne/m^3)	7.85	8.00	8.00	2.66	1.28
Yield stress (MPa)	355	205	175	145	55
Ultimate strength (MPa)	490	520	480	290	-
Thermal conductivity (W/m K)	59.00	9.40	9.40	117.00	0.19
Thermal expansion (mm/K)	1.2×10^{-5}	1.8×10^{-5}	1.8×10^{-5}	2.23×10^{-5}	2.2×10^{-5}
Specific heat (mJ/tonne K)	4.86×10^{8}	5.00×10^{8}	5.00×10^{8}	9.00×10^{8}	1.67×10^{9}

4.2. Load and Boundary Conditions

Figure 5 shows the load and boundary conditions considered for the target tank. For the outer tank, the atmospheric pressure and temperature were applied. For the inner tank, the internal pressure and LNG temperature were considered. As the design internal pressure was not a fixed value, predetermined load cases for the internal pressure by the IGC were considered in the FE model. The thermal load, calculated via heat transfer analysis to consider the atmospheric temperature and LNG operating temperature, was additionally applied in the structural analyses. A fixed boundary condition was applied to the lower section of the saddle to consider the weld attachment between the lower section of the saddle and the hull.

Table 3 summarizes the load cases determined based on the IGC code for the structural analysis performed in this study. Applied load cases are marked with a circle. The calculated maximum design accelerations for the longitudinal, transverse, and vertical directions were applied to the tank FE model. The internal liquid pressure caused by the acceleration is presented in Section 6. In addition, the heeled and collision conditions were applied. In the heeled condition, it was assumed that the tank was tilted at 30°. For the collision condition, because the tank is symmetric in the front and rear sides, double the gravitational acceleration acting in the forward direction was assumed based on KR rules for conservative purposes [17]. A design filling ratio of 85% was used in the analyses. The resultant pressures for dynamic conditions are summarized in Table 4.

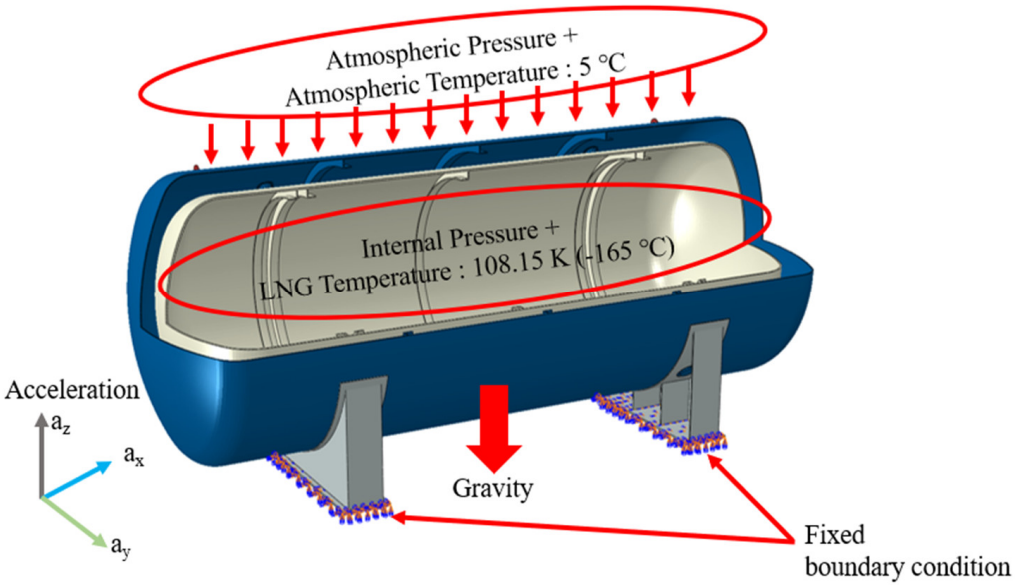

Figure 5. Load and boundary condition for target FE model.

Table 3. Load cases for structural analysis.

Load			Load Cases				
			Acc. Longi.	Acc. Trans.	Acc. Vertical	30° Heeled Condition	Collision
LNG Temp. (−165 °C)			○	○	○	○	○
Self-weight (gravity 1.0 G)			○	○	○	○	○
Vapor pressure "P_0"			○	○	○	○	○
Heeling (30°)			-	-	-	○	-
Internal liquid pressure "P_{gd}"	Liquid static pressure "P_s"		○	○	○	○	○
	Dynamic pressure "P_d"	Acc. Longi.	○	-	-	-	-
		Acc. Trans.	-	○	-	-	-
		Acc. Vertical	-	-	○	-	-
		Collision	-	-	-	-	○

Table 4. Resultant pressure for the load cases.

Load Cases	Vapor Pressure (MPa)	Internal Pressure (MPa)	Total Pressure for FEA (MPa)
Acc. Longi.	1.1	0.0011	1.1011
Acc. Trans.		0.0050	1.1050
Acc. Vertical		0.0024	1.1024
Collision		0.0047	1.1047

5. Heat Transfer Analysis

Prior to the structural analysis, heat transfer analysis was performed to consider the thermal stress of the LNG tank and surrounding structures owing to the temperature difference. The interior of the inner tank, which was in direct contact with LNG, was set to −165 °C, which is the design temperature, whereas the external temperature was set to 5 °C based on the IGC code. Because the thermal conductivities of SUS304 and SUS304L were the same, heat transfer analysis was performed for SUS304 and AL-5083-O. Figures 6 and 7 show the heat transfer analysis results of the inner tank for SUS304 and AL-5083-O, respectively. Temperature distributions of the outer tank for SUS304 and AL-5083-O are presented in Figure 8. Because the inner and outer tanks were connected via Bakelite supports, whose thermal conductivity was extremely low, and the empty space

between the inner and outer tanks was a vacuum, the temperature change in the structure around the inner tank was insignificant in both cases. Figure 9 shows the temperature changes inside the Bakelite support. The temperature distribution of the Bakelite support was identical for both SUS304 and AL-5083-O, as the outer tank was in direct contact with the inner tank. Therefore, the thermal effect due to the temperature difference in this study is not expected to be significant, as shown in Figure 10.

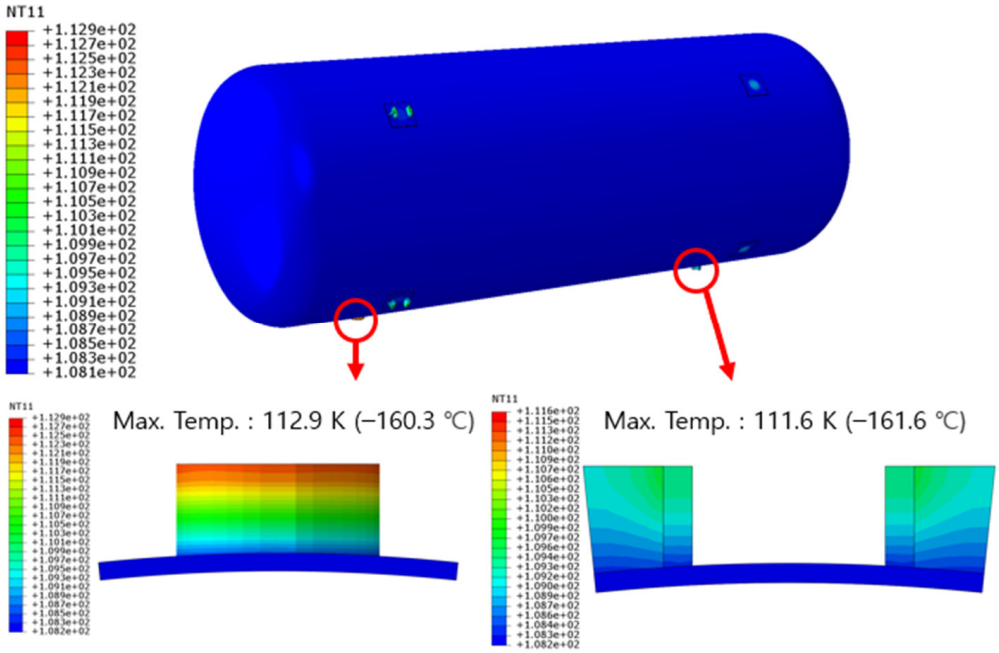

Figure 6. Temperature distribution of inner tank (SUS304).

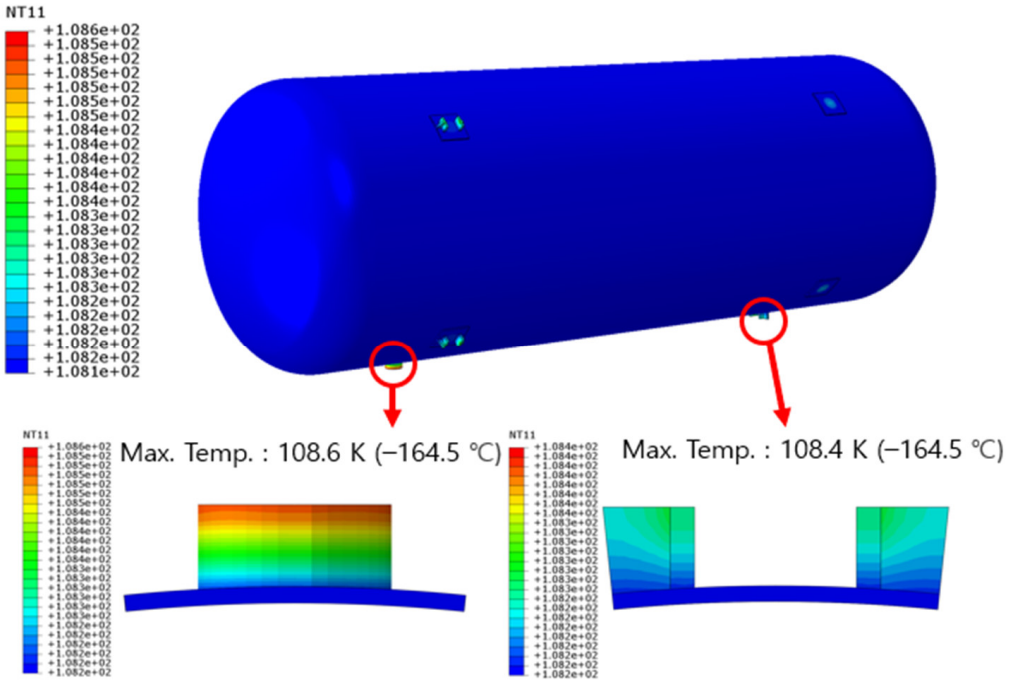

Figure 7. Temperature distribution of inner tank (AL-5083-O).

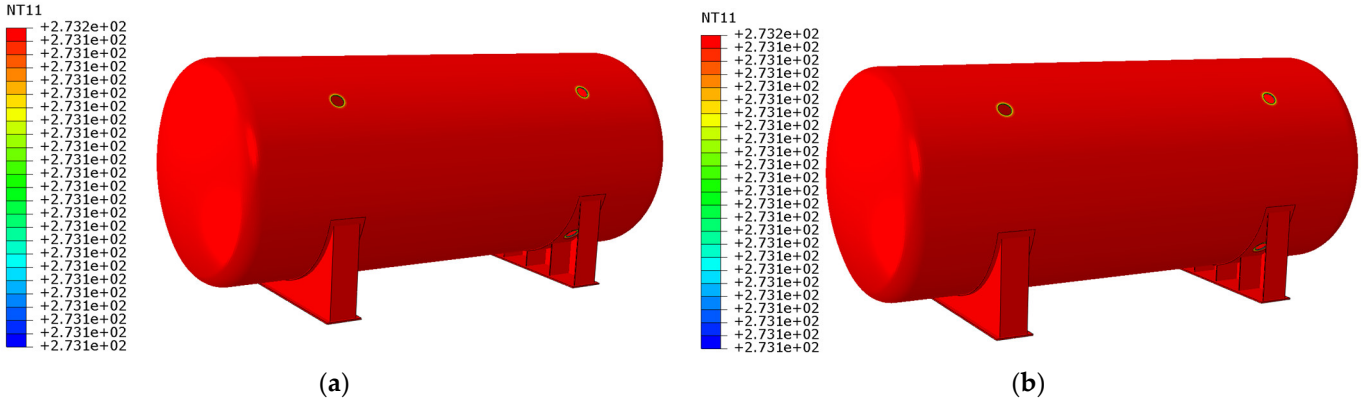

Figure 8. Temperature distribution of outer tank: (**a**) SUS304; (**b**) AL-5083-O.

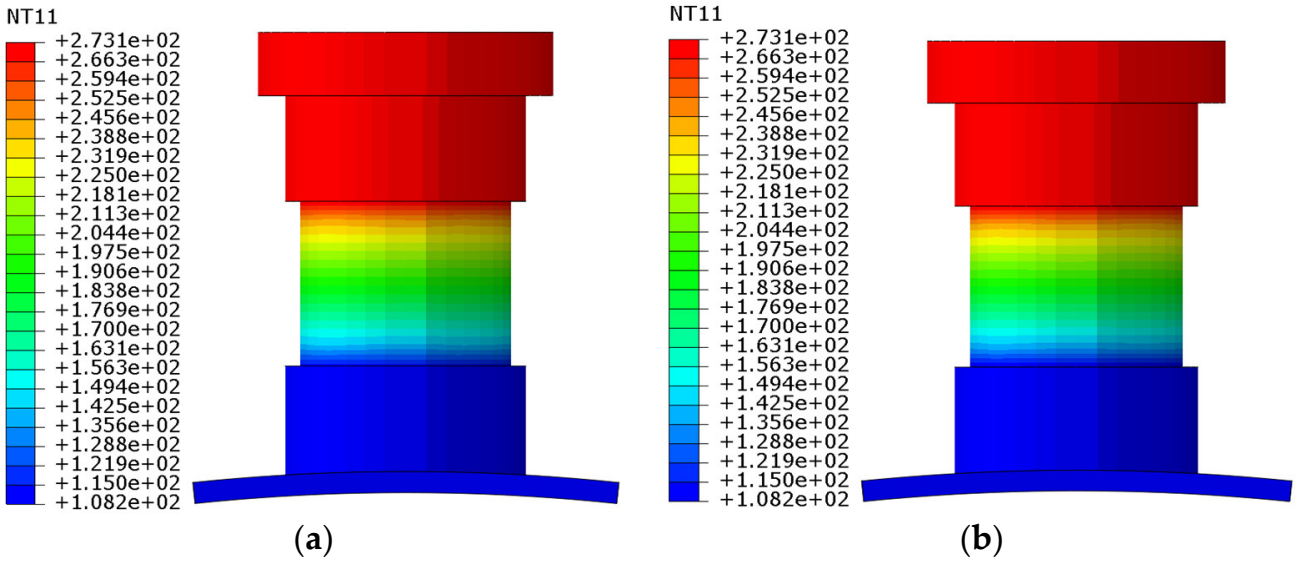

Figure 9. Temperature distribution of Bakelite support: (**a**) SUS304; (**b**) AL-5083-O.

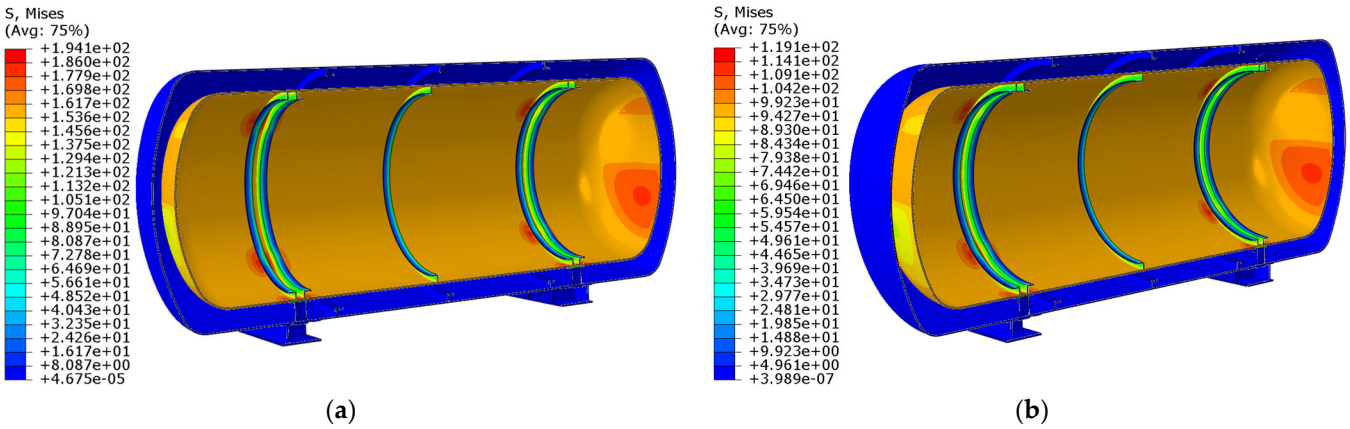

Figure 10. Thermal stress distribution of LNG fuel tank: (**a**) SUS304; (**b**) AL-5083-O.

6. Structural Analysis

6.1. Liquid Pressure Calculation

The IGC code considers fracture mechanics and crack propagation theory, in addition to the existing pressure vessel design formula, for the design of the type-C tanks. The minimum design steam pressure applied to the initial design of the tank is calculated using

Equation (1). Considering the dynamic stress against 10^8 wave encounters in the equation, the cracks do not propagate to more than half of the shell thickness during the service life of the tank. Therefore, secondary barriers are not required in type-C tanks.

$$\begin{aligned} P_0 &= 0.2 + \delta' C(\rho r)^{1.5} \\ \delta' &= 0.00185\left(\frac{\sigma_m}{\Delta\sigma_A}\right)^2, \end{aligned} \tag{1}$$

where C is a characteristic tank dimension; ρr is the relative cargo density at the design temperature; σ_m is the design primary membrane stress; and $\Delta\sigma_A$ is the allowable dynamic membrane stress range at a probability level of 10^8, which is 55 MPa for ferritic-pearlitic, martensitic, and austenitic steel, and 25 MPa for aluminum alloy.

The liquid pressure (P_{gd}) caused by the acceleration of the cargo due to ship motions is calculated using Equation (2). Finally, the internal design pressure (P_{ed}) at a specific location is calculated as the sum of the design's vapor pressure and internal liquid pressure, as shown in Equation (3).

$$P_{gd} = \alpha_\beta Z_\beta \left(\frac{\rho}{1.025 \times 10^5}\right) \tag{2}$$

$$P_{ed} = P_0 + P_{gd}, \tag{3}$$

where α_β is the resultant dimensionless acceleration from the gravitational and dynamic loads based on the acceleration ellipsoid (Figure 11). Z_β is the liquid height, as shown in Figure 12.

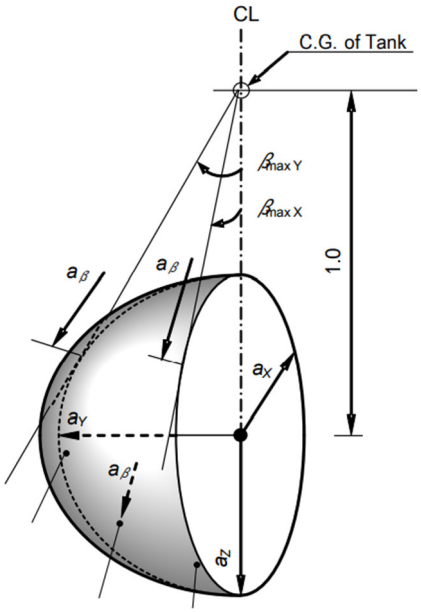

Figure 11. Acceleration ellipsoid [2].

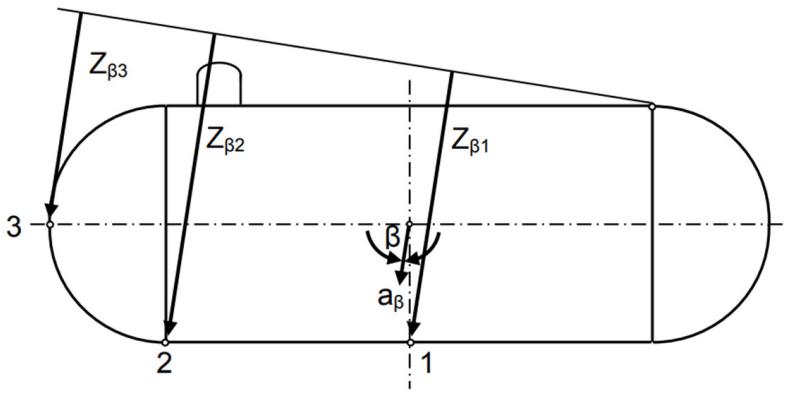

Figure 12. Determination of Z_β [2].

The maximum dimensionless accelerations (a_x, a_y, and a_z) in Figure 9 are calculated using Equations (4)–(6), respectively.

$$a_x = \pm a_0 \sqrt{0.06 + A^2 - 0.25A} \tag{4}$$

$$a_y = \pm a_0 \sqrt{0.6 + 2.5\left(\frac{x}{L} + 0.05\right)^2 + K\left(1 + 0.6K\frac{z}{B}\right)^2} \tag{5}$$

$$a_z = \pm a_0 \sqrt{1 + \left(5.3 - \frac{45}{L}\right)^2 \left(\frac{x}{L} + 0.05\right)^2 \left(\frac{0.6}{C_B}\right)^{1.5} + \left(\frac{0.6yK^{1.5}}{B}\right)^2} \tag{6}$$

$$a_0 = 0.2\frac{V}{\sqrt{L}} + \frac{34 - \frac{600}{L}}{L} \tag{7}$$

$$A = \left(0.7 - \frac{L}{1200} + 5\frac{z}{L}\right)\left(\frac{0.6}{C_B}\right) \tag{8}$$

6.2. Strength Criteria

For the design of type-C independent tanks, the calculated stresses shall not exceed the corresponding allowable stress, as follows [2]:

$$\begin{gathered} \sigma_m \le f \\ \sigma_L \le 1.5f \\ \sigma_b \le 1.5f \\ \sigma_L + \sigma_b \le 1.5f \\ \sigma_m + \sigma_b \le 1.5f \\ \sigma_m + \sigma_b + \sigma_g \le 3.0f, \end{gathered} \tag{9}$$

where σ_m is the equivalent primary general membrane stress; σ_L is the equivalent primary local membrane stress; σ_b is the equivalent primary bending stress; σ_g is the equivalent secondary stress; f is the reference allowable stress expressed as $f = min(R_m/A, R_e/B)$ as shown in Tables 5 and 6; R_m is the ultimate strength; and R_e is the yield stress.

Table 5. Design material criteria.

Material	R_e	R_m	f	$1.0f$	$1.5f$	$3.0f$	$0.9R_e$
Carbon steel (DH36)	355	490	163.3	163.3	245.0	490.0	319.5
SUS 304	205	520	136.7	136.7	205.0	410.0	184.5
SUS 304L	175	480	116.7	116.7	175.0	350.0	105.0
AL 5083-O	145	290	72.5	72.5	108.8	217.5	65.3

Table 6. A and B for calculation of reference allowable stress.

Parameter	Nickel Steels and Carbon–Manganese Steels	Austenitic Steel	Aluminum Alloy
A	3.0	3.5	4.0
B	1.5	1.5	1.5

6.3. Strength Analysis Results and Discussion

The structural strength of the type-C tank constructed using each material was evaluated under the maximum acceleration condition, 30° heeled condition, and collision condition, and the detailed results for each material are presented in Tables A1–A3 of the Appendix A, respectively. The structural evaluations for SUS304 and AL-5083-O satisfied the minimum requirement. Figures 13 and 14 show the stress contours under the transverse acceleration condition, which indicated the highest stress among the load conditions. Table 7 summarizes the results of the structural analysis. The sum of the local, bending, and secondary stresses ($\sigma_L + \sigma_b + \sigma_g$), which is the most critical condition, is shown together with the corresponding allowable stress. The calculated stress levels for SUS304

and SUS304L were identical to each other as their elastic moduli were the same, whereas the allowable stresses for the two cases were different, as the yield and tensile strengths of SUS304 and SUS304L were different. Figure 15 shows a comparison of the results presented in Table 6 for each material, where the normalized stress as the ratio of the calculated stress to the allowable stress is presented and compared in a bar chart. As shown, the normalized stress of SUS304L was the highest, although it satisfied the allowable stress under all conditions. In addition, AL-5083-O exhibited a slightly lower stress than SUS304L and had a margin of 10% or more for the acceptance criterion. Because it was confirmed that each material possessed sufficient structural safety, it was assumed that the material could be selected according to its intended purpose by considering the advantages/disadvantages of each material mentioned in the Introduction. In particular, it was found that when AL-5083-O is used, additional economic benefits can be expected because it offers significant benefits such as weight reduction and an increase in cargo capacity.

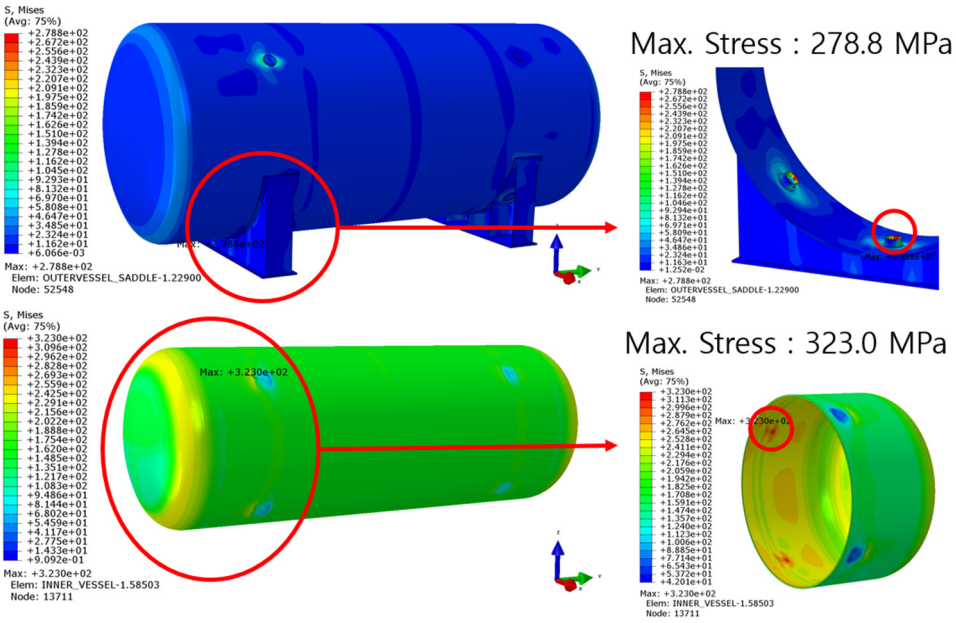

Figure 13. Stress contour of strength evaluation in transverse acceleration (SUS304).

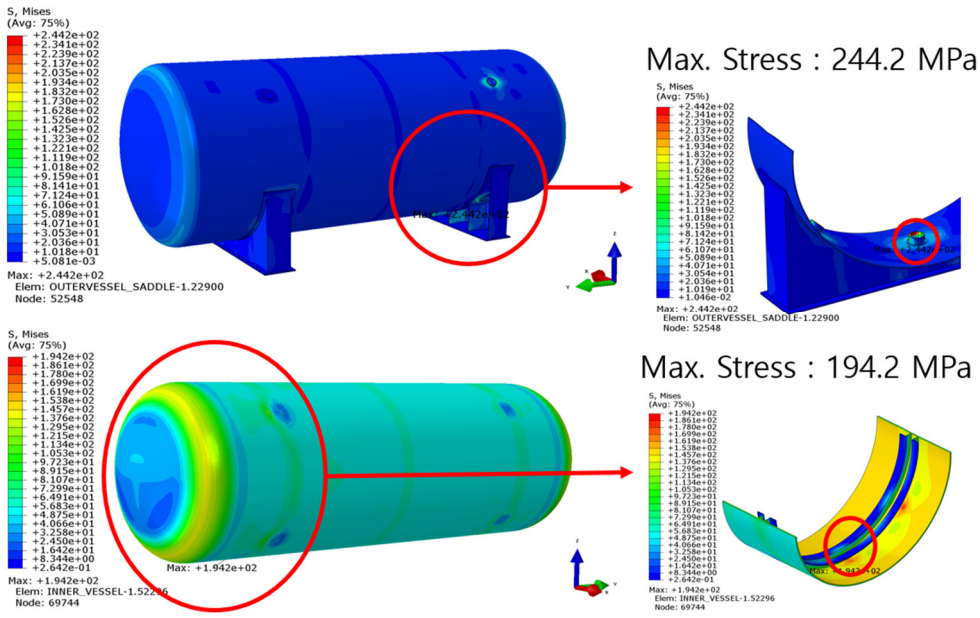

Figure 14. Stress contour of strength evaluation in transverse acceleration (AL-5083-O).

Table 7. Summary of structural analysis results.

Material		Max. Stress (MPa)		
		SUS304	**SUS304L**	**AL 5083-O**
Load case	Acc. Longi.	298.5	298.5	174.8
	Acc. Trans.	323.0	323.0	194.2
	Acc. Vertical	315.9	315.9	174.8
	30° Heel	292.5	292.5	169.8
	Collision	315.5	315.5	183.9
Allowable stress (3.0f)		410	350	217.5

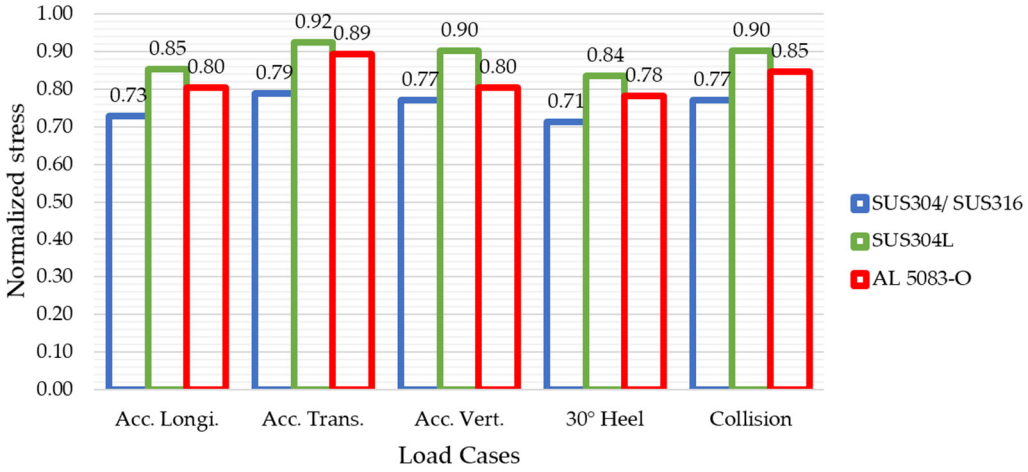

Figure 15. Comparison of normalized stresses for different materials.

7. Fatigue Analysis

As the LNG fuel tank is subjected to repeated loads under cryogenic conditions during operation or bunkering, fatigue evaluation is essential. In this study, the high-cycle fatigue caused by waves encountered during normal operations and the low-cycle fatigue damage caused by bunkering were evaluated.

Based on the IGC code, the cumulative fatigue damage was evaluated using Equation (10). In this study, 0.1 was considered as the maximum allowable cumulative fatigue damage ratio (C_w) because the detection of crack or defect development cannot be assured in the inner tank area. In Equation (10), the first term $\sum \frac{n_i}{N_i}$ and second term $\frac{n_{Loading}}{N_{Loading}}$ are associated with the high and low-cycle fatigue, respectively.

$$\sum \frac{n_i}{N_i} + \frac{n_{Loading}}{N_{Loading}} \leq C_w, \tag{10}$$

where n_i is the number of stress cycles at each stress level during the life of the tank; N_i is the number of cycles to fracture for the respective stress level based on the S–N curve in Figure 16; $n_{Loading}$ is the number of loading and unloading cycles during the life of the tank; and $N_{Loading}$ is the number of cycles to fracture for the fatigue loads due to loading and unloading.

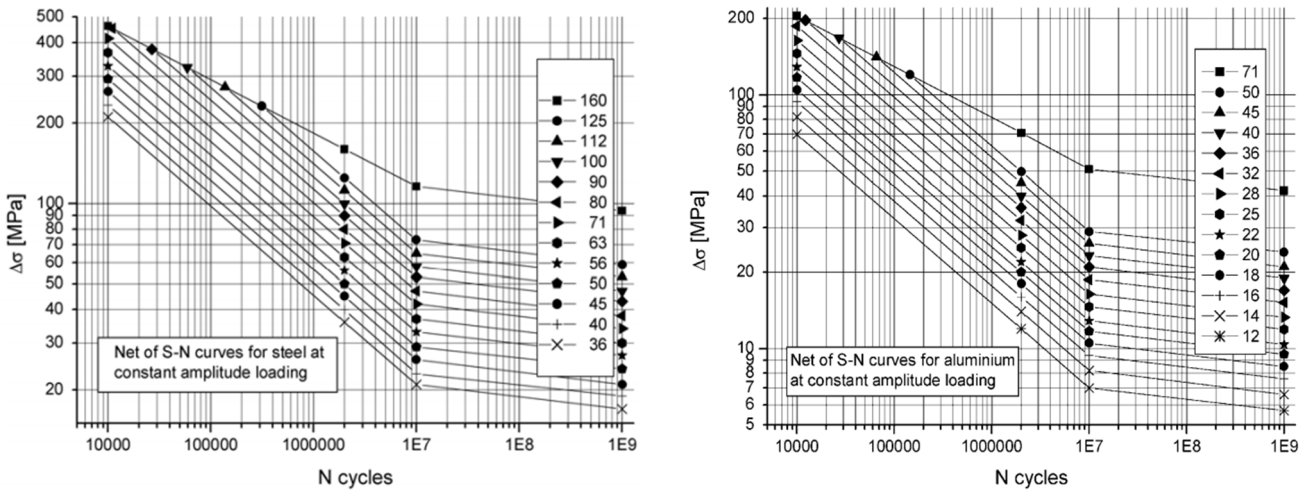

(**a**) (**b**)

Figure 16. S–N curves applied in this study: (**a**) steel; (**b**) aluminum [20].

7.1. High-Cycle Fatigue Analysis

Fatigue loads under normal operating conditions are caused by ship motions on waves. Therefore, the accelerations (longitudinal, transverse, and vertical) of the tank calculated based on the IGC code were applied to the FE model, and the resulting stress was used to evaluate the fatigue damage. If the stress is calculated by applying an acceleration of 10^8 probability, then the stress to be applied to the fatigue analysis and the corresponding number of cycles can be derived from Figure 17. Therefore, eight fatigue loads and their frequency of occurrence were derived, and high-cycle fatigue damage was calculated by adding up each fatigue damage level.

$$\begin{aligned} \sigma_i &= \tfrac{17-2\times i}{16}\sigma_{max} \\ n_i &= 0.9 \times 10^i, \end{aligned} \tag{11}$$

where i = 1, 2, 3, ... , 8.

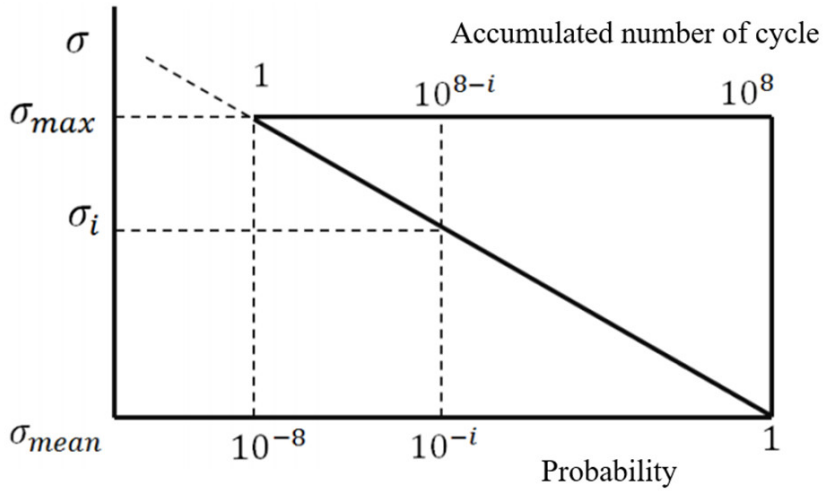

Figure 17. Calculation of fatigue stress and number of cycles [17].

The fatigue calculation was performed by applying the accelerations calculated using Equations (4)–(6). Because the elastic modulus and fatigue strength of SUS304 and SUS304L are the same, only the fatigue evaluation of SUS304 was performed, and a separate fatigue evaluation for the case involving aluminum was performed to compare the fatigue damages.

To perform an appropriate fatigue evaluation, three locations that indicated the highest stress levels were selected via a screening fatigue assessment for each loading condition. The target locations for the fatigue evaluation were created via full-penetration welding; however, FAT71 for SUS304 and FAT22 for AL-5083-O, which are typically applied for root crack applications and exhibit conservative S–N curves, were considered in this study. Figure 18 shows the maximum dynamic stress contours against the longitudinal acceleration loading conditions for SUS304/SUS304L and AL-5083-O.

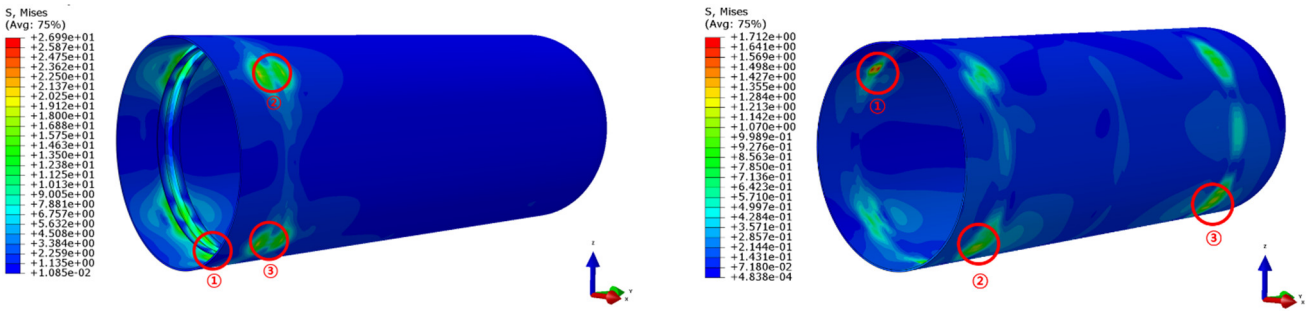

(**a**) (**b**)

Figure 18. Stress contour in longitudinal acceleration condition for fatigue evaluation: (**a**) SUS304; (**b**) AL-5083-O.

7.2. Low-Cycle Fatigue Analysis

LNG fuel tanks undergo extreme temperature differences during bunkering. When LNG is loaded and unloaded at −163 °C, thermal stress occurs in the inner tank and the surrounding area owing to temperature difference. Even though the number of LNG loading and unloading cases is insignificant compared with the entire design lifetime, the resultant stress amount due to the event may be high; therefore, low-cycle fatigue due to high stress levels should be evaluated. Low-cycle fatigue strength is typically evaluated for highly stressed areas under cyclic static loads. In this study, a filling level of 85% was assumed as the full-load condition.

The stress amplitude based on the full-load and empty conditions was considered to perform a low-cycle fatigue assessment, and the total number of loading/unloading cases based on the design life was set to 1000 (based on the IGC code). As shown in Figure 19, fatigue analysis was performed on three locations with the most significant stress difference. Even though full penetration welding was applied to the target location, FAT 71 for SUS304/SUS304L and FAT 22 for AL-5083-O were considered to evaluate fatigue life conservatively.

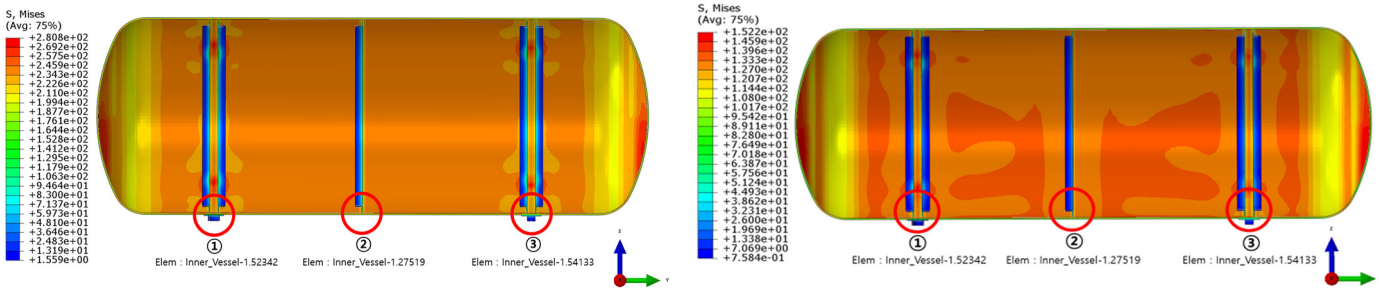

(**a**) (**b**)

Figure 19. Stress contour in full-load condition for fatigue evaluation: (**a**) SUS304; (**b**) AL-5083-O.

7.3. Fatigue Analysis Results and Discussion

Table 8 summarizes the results of the high and low-cycle fatigue cases presented in Sections 7.1 and 7.2, respectively. For both the SUS304/SUS304L and AL-5083-O cases, the

fatigue damage was insignificant. For SUS304 under transverse acceleration, a relatively large stress range was calculated, but the damage was only 5.17×10^{-7}. For the type-C tank, the design steam pressure applied to the structural design was the most dominant; therefore, it was assumed that the dynamic pressure did not contribute to a high dynamic stress. By contrast, the low-cycle fatigue that occurred during bunkering resulted in a relatively large stress range, and in the case of AL-5083-O, a fatigue damage of 6.98×10^{-3} was calculated. However, the fatigue margin was sufficient as compared with the acceptance criterion of 0.1. Comparing SUS304 and AL-5083-O, as shown in Figure 20, AL-5083-O indicated significant fatigue damage in the low cycle.

Table 8. Summary of fatigue analysis results.

Material	Load Case		Stress Range (MPa)	$N_{Loading}$	$n_{Loading}$	Fatigue Damage
SUS304	High cycle	Acc. Longi.	3.45	-	-	1.54×10^{-27}
		Acc. Trans.	29.6	-	-	5.17×10^{-7}
		Acc. Vert.	6.1	-	-	1.93×10^{-12}
	Low cycle	Bunkering	47.8	2.29×10^{6}	1000	4.38×10^{-4}
AL 5083-O	High cycle	Acc. Longi.	1.12	-	-	1.02×10^{-29}
		Acc. Trans.	8.62	-	-	3.25×10^{-10}
		Acc. Vert.	2.24	-	-	4.28×10^{-23}
	Low cycle	Bunkering	48.2	1.43×10^{5}	1000	6.98×10^{-3}

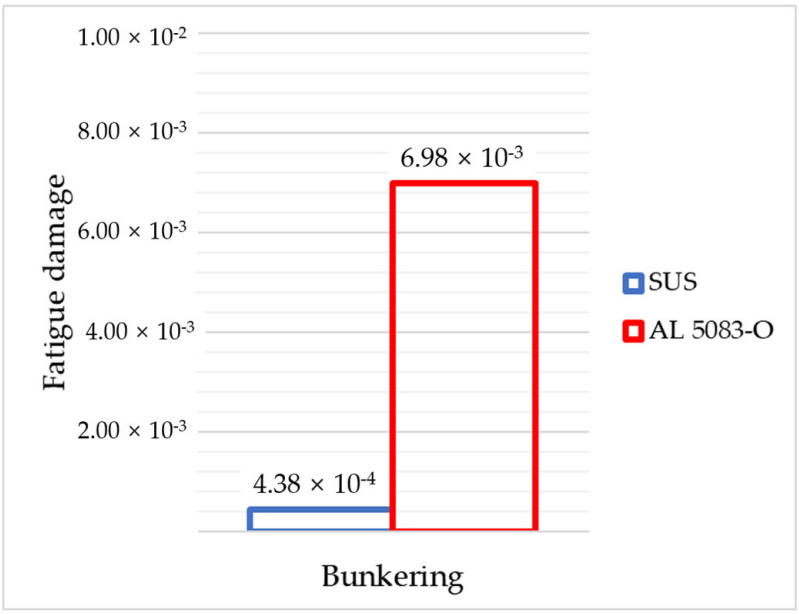

Figure 20. Comparison of low fatigue damage ratios based on different materials.

8. Conclusions

In this study, heat transfer analysis, structural analysis, and fatigue analysis, for various conditions, were performed based on the IGC code for the structural integrity assessment of an independent type-C cylindrical tank. In addition, case studies were conducted on SUS304/SUS304L and AL-5083-O, which are typically used for LNG tank applications, to evaluate their applicability. Based on the results of this study, the following conclusions were obtained:

- Heat transfer analysis was performed to consider the thermal effects due to the LNG operating temperature on the ultimate strength. The resultant temperature change in the tank and the surrounding structural members was insignificant because of the

Bakelite support used as insulation and the vacuum between the inner and outer tanks. Furthermore, the thermal effect was also insignificant.

- Structural analysis considering the maximum accelerations (longitudinal, transverse, and vertical), 30° heeled, and collision conditions, based on the IGC code, was performed. The analysis results showed that the tanks constructed using SUS304/304L and AL-5083-O satisfied all acceptance criteria of the IGC code. The safety margin for the ultimate capacity of AL-5083-O was higher than that of SUS304L.
- Fatigue analysis was performed based on the dynamic load experienced during normal operation and bunkering. Both SUS304 and AL-5083-O applied to the analysis indicated that the high and low-cycle fatigue damages were insignificant as compared with the acceptance criteria. The low-cycle fatigue case indicated more severe damage compared with the high-cycle fatigue case; however, it still indicated a sufficient fatigue margin.
- Structural integrity evaluations based on the IGC requirements were performed on SUS304/304L and AL-5083-O, which are widely used in LNG tank applications, and all the cases satisfied the corresponding minimum criteria. Therefore, they can be selected based on their purpose and advantages/disadvantages. In particular, additional economic benefits can be expected when AL-5083-O is used, which affords weight reduction and an increase in cargo capacity.

Author Contributions: Conceptualization, Y.-I.P.; methodology, Y.-I.P.; validation, Y.-I.P.; formal analysis, J.-S.C.; investigation, J.-H.K.; writing—original draft preparation, J.-H.K.; writing—review and editing, Y.-I.P.; visualization, J.-S.C.; supervision, Y.-I.P.; project administration, Y.-I.P.; funding acquisition, Y.-I.P. All authors have read and agreed to the published version of the manuscript.

Funding: This work was supported by the Dong-A University research fund.

Institutional Review Board Statement: Not applicable.

Informed Consent Statement: Not applicable.

Data Availability Statement: The data presented in this study are available on request from the corresponding author.

Conflicts of Interest: The authors declare no conflict of interest.

Appendix A

Table A1. Summary of structural analysis result for SUS304.

Load Case		Part	Acceptance Criteria (MPa)										Judge.
			σ_m (1.0f)		σ_L (1.5f)		$\sigma_L + \sigma_b$ (1.5f)		$\sigma_L + \sigma_b + \sigma_g$ (3.0f)		σ_{allow}		
			Cal.	Allow.	Cal.	Allow.	Cal.	Allow.	Cal.	Allow.	Cal.	Allow.	
Acc. Longi.	Inner	Shell and head	86.9	136.7	56.8	205.0	58.7	205.0	298.5	410.0	-	-	OK
		Stifferner	-	-	68.8	205.0	79.5	205.0	266.3	410.0	-	-	OK
		Pad	-	-	29.6	205.0	42.9	205.0	192.1	410.0	-	-	OK
		Support Guide	-	-	9.5	205.0	17.4	205.0	76.6	410.0	-	-	OK
	Outer	Shell and head	46.3	163.3	18.6	245.0	61.7	245.0	56.1	490.0	-	-	OK
		Stifferner	-	-	-	-	-	-	-	-	23.9	163.3	OK
		Saddle	-	-	-	-	-	-	-	-	73.0	163.3	OK
Acc. Trans.	Inner	Shell and head	87.6	136.7	33.6	205.0	90.5	205.0	323.0	410.0	-	-	OK
		Stifferner	-	-	92.3	205.0	106.9	205.0	288.5	410.0	-	-	OK
		Pad	-	-	64.8	205.0	126.4	205.0	225.1	410.0	-	-	OK
		Support Guide	-	-	145.1	205.0	189.5	205.0	188.4	410.0	-	-	OK
	Outer	Shell and head	46.2	163.3	50.2	245.0	156.0	245.0	113.6	490.0	-	-	OK
		Stifferner	-	-	-	-	-	-	-	-	237.2	163.3	OK
		Saddle	-	-	-	-	-	-	-	-	134.5	163.3	OK

Table A1. *Cont.*

Load Case		Part	Acceptance Criteria (MPa)										Judge.
			σ_m (1.0f)		σ_L (1.5f)		$\sigma_L + \sigma_b$ (1.5f)		$\sigma_L + \sigma_b + \sigma_g$ (3.0f)		σ_{allow}		
			Cal.	Allow.	Cal.	Allow.	Cal.	Allow.	Cal.	Allow.	Cal.	Allow.	
Acc. Vert.	Inner	Shell and head	87.7	136.7	36.9	205.0	73.9	205.0	315.9	410.0	-	-	OK
		Stifferner	-	-	68.8	205.0	79.8	205.0	285.1	410.0	-	-	OK
		Pad	-	-	27.5	205.0	48.2	205.0	211.6	410.0	-	-	OK
		Support Guide	-	-	20.5	205.0	22.8	205.0	83.4	410.0	-	-	OK
	Outer	Shell and head	47.3	163.3	36.3	245.0	72.8	245.0	86.6	490.0	-	-	OK
		Stifferner	-	-	-	-	-	-	-	-	27.3	163.3	OK
		Saddle	-	-	-	-	-	-	-	-	124.2	163.3	OK
30° Heel	Inner	Shell and head	88.2	136.7	58.4	205.0	61.2	205.0	292.5	410.0	-	-	OK
		Stifferner	-	-	17.8	205.0	20.1	205.0	267.9	410.0	-	-	OK
		Pad	-	-	22.9	205.0	53.1	205.0	204.5	410.0	-	-	OK
		Support Guide	-	-	23.2	205.0	48.0	205.0	85.5	410.0	-	-	OK
	Outer	Shell and head	45.1	163.3	23.3	245.0	85.4	245.0	66.8	490.0	-	-	OK
		Stifferner	-	-	-	-	-	-	-	-	19.7	163.3	OK
		Saddle	-	-	-	-	-	-	-	-	67.7	163.3	OK
Collision	Inner	Shell and head	89.1	136.7	39.6	205.0	81.6	205.0	315.5	410.0	-	-	OK
		Stifferner	-	-	149.2	205.0	174.0	205.0	282.6	410.0	-	-	OK
		Pad	-	-	36.2	205.0	47.7	205.0	182.4	410.0	-	-	OK
		Support Guide	-	-	83.9	205.0	101.0	205.0	110.7	410.0	-	-	OK
	Outer	Shell and head	61.0	163.3	41.1	245.0	158.8	245.0	131.2	490.0	-	-	OK
		Stifferner	-	-	-	-	-	-	-	-	216.7	163.3	OK
		Saddle	-	-	-	-	-	-	-	-	93.1	163.3	OK

Table A2. Summary of structural analysis result for SUS304L.

Load Case		Part	Acceptance Criteria (MPa)										Judge.
			σ_m (1.0f)		σ_L (1.5f)		$\sigma_L + \sigma_b$ (1.5f)		$\sigma_L + \sigma_b + \sigma_g$ (3.0f)		σ_{allow}		
			Cal.	Allow.	Cal.	Allow.	Cal.	Allow.	Cal.	Allow.	Cal.	Allow.	
Acc. Longi.	Inner	Shell and head	86.9	116.7	56.8	175.0	58.7	175.0	298.5	350.0	-	-	OK
		Stifferner	-	-	68.8	175.0	79.5	175.0	266.3	350.0	-	-	OK
		Pad	-	-	29.6	175.0	42.9	175.0	192.1	350.0	-	-	OK
		Support Guide	-	-	9.5	175.0	17.4	175.0	76.6	350.0	-	-	OK
	Outer	Shell and head	46.3	163.3	18.6	245.0	61.7	245.0	56.1	490.0	-	-	OK
		Stifferner	-	-	-	-	-	-	-	-	23.9	163.3	OK
		Saddle	-	-	-	-	-	-	-	-	73.0	163.3	OK
Acc. Trans.	Inner	Shell and head	87.6	116.7	33.6	175.0	90.5	175.0	323.0	350.0	-	-	OK
		Stifferner	-	-	92.3	175.0	106.9	175.0	288.5	350.0	-	-	OK
		Pad	-	-	64.8	175.0	126.4	175.0	225.1	350.0	-	-	OK
		Support Guide	-	-	145.1	175.0	169.5	175.0	188.4	350.0	-	-	OK
	Outer	Shell and head	46.2	163.3	50.2	245.0	156.0	245.0	113.6	490.0	-	-	OK
		Stifferner	-	-	-	-	-	-	-	-	237.2	163.3	OK
		Saddle	-	-	-	-	-	-	-	-	134.5	163.3	OK
Acc. Vert.	Inner	Shell and head	87.7	116.7	36.9	175.0	73.9	175.0	315.9	350.0	-	-	OK
		Stifferner	-	-	68.8	175.0	79.8	175.0	285.1	350.0	-	-	OK
		Pad	-	-	27.5	175.0	48.2	175.0	211.6	350.0	-	-	OK
		Support Guide	-	-	20.5	175.0	22.8	175.0	83.4	350.0	-	-	OK
	Outer	Shell and head	47.3	163.3	36.3	245.0	72.8	245.0	86.6	490.0	-	-	OK
		Stifferner	-	-	-	-	-	-	-	-	27.3	163.3	OK
		Saddle	-	-	-	-	-	-	-	-	124.2	163.3	OK
30° Heel	Inner	Shell and head	88.2	116.7	58.4	175.0	61.2	175.0	292.5	350.0	-	-	OK
		Stifferner	-	-	17.8	175.0	20.1	175.0	267.9	350.0	-	-	OK
		Pad	-	-	22.9	175.0	53.1	175.0	204.5	350.0	-	-	OK
		Support Guide	-	-	23.2	175.0	48.0	175.0	85.5	350.0	-	-	OK
	Outer	Shell and head	45.1	163.3	23.3	245.0	85.4	245.0	66.8	490.0	-	-	OK
		Stifferner	-	-	-	-	-	-	-	-	19.7	163.3	OK
		Saddle	-	-	-	-	-	-	-	-	67.7	163.3	OK

Table A2. *Cont.*

Load Case		Part	Acceptance Criteria (MPa)										Judge.
			σ_m (1.0f)		σ_L (1.5f)		$\sigma_L + \sigma_b$ (1.5f)		$\sigma_L + \sigma_b + \sigma_g$ (3.0f)		σ_{allow}		
			Cal.	Allow.	Cal.	Allow.	Cal.	Allow.	Cal.	Allow.	Cal.	Allow.	
Collision	Inner	Shell and head	89.1	116.7	39.6	175.0	81.6	175.0	315.5	350.0	-	-	OK
		Stifferner	-	-	149.2	175.0	174.0	175.0	282.6	350.0	-	-	OK
		Pad	-	-	36.2	175.0	47.7	175.0	182.4	350.0	-	-	OK
		Support Guide	-	-	83.9	175.0	101.0	175.0	110.7	350.0	-	-	OK
	Outer	Shell and head	61.0	163.3	41.1	245.0	158.8	245.0	131.2	490.0	-	-	OK
		Stifferner	-	-	-	-	-	-	-	-	216.7	163.3	OK
		Saddle	-	-	-	-	-	-	-	-	93.1	163.3	OK

Table A3. Summary of structural analysis result for AL-5083-O.

Load Case		Part	Acceptance Criteria (MPa)										Judge.
			σ_m (1.0f)		σ_L (1.5f)		$\sigma_L + \sigma_b$ (1.5f)		$\sigma_L + \sigma_b + \sigma_g$ (3.0f)		σ_{allow}		
			Cal.	Allow.	Cal.	Allow.	Cal.	Allow.	Cal.	Allow.	Cal.	Allow.	
Acc. Longi.	Inner	Shell and head	63.0	72.5	58.0	108.8	59.3	108.8	174.8	217.5	-	-	OK
		Stifferner	-	-	66.7	108.8	70.5	108.8	145.8	217.5	-	-	OK
		Pad	-	-	19.6	108.8	33.5	108.8	73.4	217.5	-	-	OK
		Support Guide	-	-	19.0	108.8	19.7	108.8	32.5	217.5	-	-	OK
	Outer	Shell and head	46.4	163.3	16.0	245.0	50.4	245.0	55.8	490.0	-	-	OK
		Stifferner	-	-	-	-	-	-	-	-	216.4	319.5	OK
		Saddle	-	-	-	-	-	-	-	-	55.1	319.5	OK
Acc. Trans.	Inner	Shell and head	63.8	72.5	35.9	108.8	80.4	108.8	194.2	217.5	-	-	OK
		Stifferner	-	-	81.3	108.8	86.7	108.8	164.2	217.5	-	-	OK
		Pad	-	-	25.7	108.8	59.7	108.8	104.8	217.5	-	-	OK
		Support Guide	-	-	86.5	108.8	86.5	108.8	84.4	217.5	-	-	OK
	Outer	Shell and head	46.2	163.3	35.4	245.0	148.7	245.0	98.0	490.0	-	-	OK
		Stifferner	-	-	-	-	-	-	-	-	235.3	319.5	OK
		Saddle	-	-	-	-	-	-	-	-	115.8	319.5	OK
Acc. Vert.	Inner	Shell and head	63.9	72.5	34.2	108.8	55.8	108.8	174.8	217.5	-	-	OK
		Stifferner	-	-	58.7	108.8	67.6	108.8	152.8	217.5	-	-	OK
		Pad	-	-	29.4	108.8	42.9	108.8	78.3	217.5	-	-	OK
		Support Guide	-	-	13.3	108.8	16.4	108.8	36.5	217.5	-	-	OK
	Outer	Shell and head	45.9	163.3	26.6	245.0	52.4	245.0	62.3	490.0	-	-	OK
		Stifferner	-	-	-	-	-	-	-	-	22.2	319.5	OK
		Saddle	-	-	-	-	-	-	-	-	90.0	319.5	OK
30° Heel	Inner	Shell and head	64.6	72.5	58.0	108.8	59.7	108.8	169.8	217.5	-	-	OK
		Stifferner	-	-	64.7	108.8	68.5	108.8	150.5	217.5	-	-	OK
		Pad	-	-	29.2	108.8	41.8	108.8	82.3	217.5	-	-	OK
		Support Guide	-	-	18.0	108.8	21.5	108.8	41.4	217.5	-	-	OK
	Outer	Shell and head	44.8	163.3	17.7	245.0	63.8	245.0	54.5	490.0	-	-	OK
		Stifferner	-	-	-	-	-	-	-	-	18.6	319.5	OK
		Saddle	-	-	-	-	-	-	-	-	54.6	319.5	OK
Collision	Inner	Shell and head	64.5	72.5	35.7	108.8	49.0	108.8	183.9	217.5	-	-	OK
		Stifferner	-	-	107.3	108.8	125.8	108.8	162.5	217.5	-	-	OK
		Pad	-	-	29.4	108.8	37.7	108.8	74.5	217.5	-	-	OK
		Support Guide	-	-	46.5	108.8	80.7	108.8	83.7	217.5	-	-	OK
	Outer	Shell and head	59.2	163.3	110.7	245.0	118.1	245.0	101.9	490.0	-	-	OK
		Stifferner	-	-	-	-	-	-	-	-	84.3	319.5	OK
		Saddle	-	-	-	-	-	-	-	-	149.7	319.5	OK

References

1. Englert, D.; Losos, A.; Raucci, C.; Smith, T. *The Role of LNG in the Transition Toward Low- and Zero-Carbon Shipping*; World Bank: Washington, DC, USA, 2021. [CrossRef]
2. IMO. *MSC. International Code for the Construction and Equipment of Ships Carrying Liquefied Gasses in Bulk (IGC Code)*; IMO: London, UK, 2014; Volume 391.
3. Oh, D.; Song, S.; Kim, N.; Kim, M. Effect of Cryogenic Temperature on Low-Cycle Fatigue Behavior of AISI 304L Welded Joint. *Metals* **2018**, *8*, 657. [CrossRef]
4. Niu, W.; Li, G.; Ju, Y.; Fu, Y. Design and analysis of the thermal insulation system for a new independent type B LNG carrier. *Ocean Eng.* **2017**, *142*, 51–61. [CrossRef]
5. Gupta, S.; Singh, D.; Yadav, A.; Jain, S.; Pratap, B. A comparative study of 5083 aluminium alloy and 316L stainless steel for shipbuilding material. *Mater. Today Proc.* **2020**, *28*, 2358–2363. [CrossRef]
6. De Menezes Netto, E.B.; Kliauga, A.M.; Plaut, R.L.; Padilha, A.F. A comparative study using three stainless steels types (austenitic, super-ferritic and duplex ferritic-austenitic) and three industrial nitrocarburizing processes (liquid, gaseous and plasma). In Proceedings of the 1st ASM International Surface Engineering Conference and the 13th IFHTSE Congress, Columbus, OH, USA, 7–10 October 2002.
7. Kim, T.-W.; Kim, S.-K.; Park, S.-B.; Lee, J.-M. Design of Independent Type-B LNG Fuel Tank: Comparative Study between Finite Element Analysis and International Guidance. *Adv. Mater. Sci. Eng.* **2018**, *2018*, 1–14. [CrossRef]
8. Jeong, H.-W.; Kim, T.-H.; Kim, S.-S.; Shim, W.J. Thermal analysis of insulation system for KC-1 membrane LNG tank. *J. Ocean Eng. Technol.* **2017**, *31*, 91–102.
9. Park, M.-J.; Choi, B.-K.; Kim, Y. On the efficient time domain stress analysis for the rolling chock of an independent type LNG tank targeting fatigue damage evaluation. *Mar. Struct.* **2017**, *53*, 32–51. [CrossRef]
10. Ryu, M.C.; Jung, J.H.; Kim, Y.S.; Kim, Y. Sloshing design load prediction of a membrane type LNG cargo containment system with two-row tank arrangement in offshore applications. *Int. J. Nav. Archit. Ocean. Eng.* **2016**, *8*, 1–17. [CrossRef]
11. Kim, Y. Rapid response calculation of LNG cargo containment system under sloshing load using wavelet transformation. *Int. J. Nav. Archit. Ocean. Eng.* **2013**, *5*, 227–245. [CrossRef]
12. Park, Y.I. Ultimate crushing strength criteria for GTT NO96 LNG carrier cargo containment system under sloshing load. *Ocean Eng.* **2019**, *188*, 106224. [CrossRef]
13. Park, Y.I.; Lee, J.H. Buckling strength of GTT NO96 LNG Carrier cargo containment system. *Ocean Eng.* **2018**, *154*, 43–58. [CrossRef]
14. Lin, Y.; Ye, C.; Yu, Y.-Y.; Bi, S.-W. An approach to estimating the boil-off rate of LNG in type C independent tank for floating storage and regasification unit under different filling ratio. *Appl. Therm. Eng.* **2018**, *135*, 463–471. [CrossRef]
15. Heo, K.H.; Kang, W.S.; Park, B.Q. Consideration for IMO Type C Independent Tank Rule Scantling Process and Evaluation Methods. *Spec. Issue Soc. Naval Archit. Korea* **2017**, 93–104. Available online: https://www.koreascience.or.kr/article/CFKO201729562508726.page (accessed on 13 October 2021).
16. Yao, Y.; Zhongyun, G. The structure design of type-C independent tank on LNG ship. In Proceedings of the 2015 Word Congress on Advances in Structural Engineering and Mechanics, Incheon, Korea, 25–29 August 2015.
17. Korean Register of Shipping. *International Code for the Construction and Equipment of Ships Carrying Liquefied Gases in Bulk (IGC Code)*; KR: Busan, Korea, 2014.
18. Mukhraiya, V.; Yadav, R.K.; Kori, S. Thermal conductivity analysis in various materials using composite wall apparatus. *IJMET* **2016**, *7*, 342–350.
19. Dassault Systèmes Simulia Corp. *Abaqus 6.14 Theory Manual*; Dassault Systèmes Simulia Corp.: Irving, TX, USA, 2014.
20. Hobbacher, A.F. *Recommendations for Fatigue Design of Welded Joints and Components*; Springer International Publishing: Cham, Switzerland, 2016. [CrossRef]